Optical reflectance of alkali-textured silicon wafers with pyramidal facets: 2D analytical model

Adebayo Adeboye Fashina
Department of Theoretical and Applied Physics, African University of Science and Technology, PMB 681, Garki, Abuja, Nigeria

Martiale Gaetan Zebaze Kana
Physics Advanced Laboratory, Sheda Science and Technology Complex, PMB 186, Garki, Abuja, Nigeria; and Department of Materials Science and Engineering, Kwara State University, PMB 1530, Malate, Nigeria

Winston Oluwole Soboyejo[a)]
Department of Theoretical and Applied Physics, African University of Science and Technology, PMB 681, Garki, Abuja, Nigeria; Department of Mechanical and Aerospace Engineering, Princeton University, Princeton, New Jersey 08544, USA; and Princeton Institute of Science and Technology of Materials (PRISM), Bowen Hall, Princeton, New Jersey 08544, USA

(Received 19 September 2014; accepted 17 February 2015)

This study presents an analytical model of the reflectance of flat and textured silicon substrates. The model was used to study the reflection behavior of textured silicon surfaces under non-normal incidence. By characterizing the incident light and facets of the silicon wafer with vector geometry, dot products and Phong's reflection model (https://cs.oberlin.edu/~bob/cs357.08/VectorGeometry/VectorGeometry.pdf) were used to determine the reflection angles between incident light rays and pyramidal facets. The possible optical interactions are considered for a wide range of pyramidal geometries and light incidence angles that are relevant to the exposure of textured silicon surfaces to incident sunlight. Furthermore, the model was used to investigate the possibility of secondary reflection, for the full range of incidence angles to the substrate. The textured silicon surfaces were found to reduce the reflection angles more effectively than flat substrates at lower angles of incidence. Secondary reflection was also found to be experienced or guaranteed, for all pyramid heights, when the angle of incidence to the substrate was less than 19.4°. The predictions are validated with experimental measurements of reflectance from (001)-textured silicon surfaces. The implications of the results are then discussed for the development of micropyramids for improved photoconversion in silicon solar cells.

I. INTRODUCTION

Surface texturing in solar-based devices is a geometric method of reducing reflection in crystalline silicon substrates.[1] It is often achieved by the anisotropic etching of (100)-oriented silicon substrates into square-based pyramidal structures.[2] The pyramidal structures are formed by the alkaline etching of (100)-oriented silicon surfaces along crystallographic orientations that expose the {111} planes.[3] Potassium hydroxide (KOH) and additive isopropyl alcohol (IPA) are two of the most common alkaline solutions that are used for anisotropic etching of silicon surfaces.[4–12] The sizes and uniformities of the resulting pyramids are also traceable to IPA, which acts as a wetting agent, when added to alkaline etchants.[11]

Furthermore, the pyramidal sizes, heights, and base widths are usually on the order of several micrometers.[12,13] Hence, the reflection falls within a basic structure that supports geometric optics.[14] Consequently, the surface texturing of (100)-oriented silicon substrates can be used to improve the absorption of light within the silicon substrates.[15] This can be achieved by using the reflection from micropyramids to redirect light to produce multiple reflections that increase the possibility of light absorption by silicon substrates. Since such increased absorption can enhance photocharge conversion and solar cell efficiency, there is a need to study the effects of micropyramidal geometries on the reflectance of textured silicon surfaces.

In a recent work, Baker-Finch and McIntosh[16,17] considered the reflection of normally incident light from textured silicon surfaces. They presented the reflection path and the fraction of rays that follow a given path, using geometrical approach for regular inverted pyramidal textures and a ray tracing method for random pyramidal textures.[16] They were able to establish that, for all normally incident rays that intersect a pyramidal facet, 88.9% of incident rays experience a secondary reflection, while the remaining 11.1% experience tertiary reflection.[17]

Contributing Editor: Winston Schoenfeld
[a)]Address all correspondence to this author.
e-mail: soboyejo@princeton.edu
DOI: 10.1557/jmr.2015.70

 © Materials Research Society 2015

https://doi.org/10.1557/jmr.2015.70 Published online by Cambridge University Press

However, in practice, the incident rays of sunlight are not always normal to the surfaces of textured silicon solar cells. Since the angles of incidence may vary, depending on the position on the earth, and the earth's rotation about the sun and about its own axis, there is a need to explore the possible effects of different angles of incidence on the reflection of sunlight from {111} facets on the surfaces of textured silicon solar cells. Hence, the work of Baker-Finch is limited to normal incidence, which is not always the case for most solar cells in service.

In this work, an analytical model is used to determine how incident light interacts with textured micropyramidal facets on alkali-textured silicon surfaces. The dependence of the secondary reflection on the angles of incidence of light rays is explored along with the contributions of the primary and secondary reflection to the total reflection. The possible optical interactions are considered for a range of pyramidal geometries and light incidence angles. The analytical model is then used to determine the reflectances of well controlled textured surfaces. The potential for light trapping is also explored, before discussing the implications of the results for the design of microtextured silicon surfaces.

II. MODELING

A. Pyramids on etched silicon surfaces

The silicon solar industry relies largely on silicon wafers with (100), (110), and (111) orientations.[18] However, (100) wafers are the most geometrically appealing, since the orientations of {111} planes can be easily located on them.[18] To understand the etching behavior of different wafers, it is important to know the relative positions of different crystal planes in these wafers. It is also important to know the angles that they make with each other, after etching.

During wet anisotropic etching, grooves with {111} sidewalls are exposed.[14] These are aligned with {100} planes at specific angles.[15] Also, the KOH solution is the preferred etchant that is used in the anisotropic etching of silicon to produce grooves with {111} sidewalls. This is attributed to its high anisotropy against {111} planes.[19,20] Furthermore, the angles between the individual crystallographic planes can be calculated using vector operations (dot products), since the angles between {100} and {111} planes are the same as the angles between the unit vectors of their normals. Thus, by inspection, the unit normals of both the (100) plane and the (111) plane can be obtained from their Miller indices, as shown in Fig. 1.

In an effort to demonstrate the geometrical properties of silicon crystal on a (100) plane, the dot product [Eq. (1)] is used to obtain the angle between the (111) plane indices and the (100) plane indices to be 54.74°.

$$\hat{n}_{100} \cdot \hat{n}_{111} = |\hat{n}_{100}||\hat{n}_{111}| \cos\theta \quad , \tag{1}$$

where $|\hat{n}_{100}|$ and $|\hat{n}_{111}|$ represent the magnitudes of the unit normal vectors and θ is the angle between the (111) facet and the (100) substrate.

The above angle corresponds to that specified from Wulf's stereographic projections of a (100)-oriented silicon crystal.[21] Due to symmetry of the (111) plane on the (100) plane, the (111) plane meets the (010) plane and the (001) plane at an angle of 54.74°. The intersection of the (111) plane also forms a square-based pyramid. This implies that, for all incident light rays normal to the substrate, the primary reflections are oriented at 54.74° to the substrate surfaces. However, for actual industrial c-Si solar cells, where non-ideal etching is observed, a slightly smaller base angle (or facet tilt angle) is normally observed.[16,22] This has been shown to be less than 52° in Refs. 16 and 22.

B. Textured surface model

1. Vector geometry approach

For a collimated beam of light that interacts with a textured silicon surface at a particular angle,[15] the vector geometry approach explored in this section considers the possible angles of incidence of light relative to the pyramidal {111} facets. Within this context, the vector geometry approach uses vector dot products and Phong's projection model[23] to determine the angles of the reflected rays.

Since the KOH texturing of (100) wafers forms pyramidal {111} planes,[24,25] we begin by representing the pyramidal surfaces by the vector coordinates of their plane normals. As shown in Fig. 2, the diagonals of the pyramids are represented, respectively, by unit vectors i and j, while k is the normal to the substrate. This allows us to specify the normal vector, n, for each of the facets on the pyramid (see Fig. 2).

Furthermore, the incident light ray is also defined by a vector, $v = -i + j - x \times k$ (where x is a variable). Since the normal to the substrate plane is the (001) direction, we define it as $n = k$. Thus, the dot product is used to determine the angle between v and n. This gives:

$$v \cdot n = |v||n| \cos\theta \quad , \tag{2}$$

where $|\boldsymbol{v}|$ and $|\boldsymbol{n}|$ represent the magnitudes of the vectors v and n, respectively, and θ is the angle between v and n. Hence, rearranging Eq. (2) gives:

$$\cos\theta = \frac{-x}{\sqrt{2 + x^2}} \quad . \tag{3}$$

With the light ray vector, v, known for a given angle of incidence [Eq. (3)], the angles of incidence of the primary reflection can be determined. Note that Eq. (3) applies

https://doi.org/10.1557/jmr.2015.70 Published online by Cambridge University Press

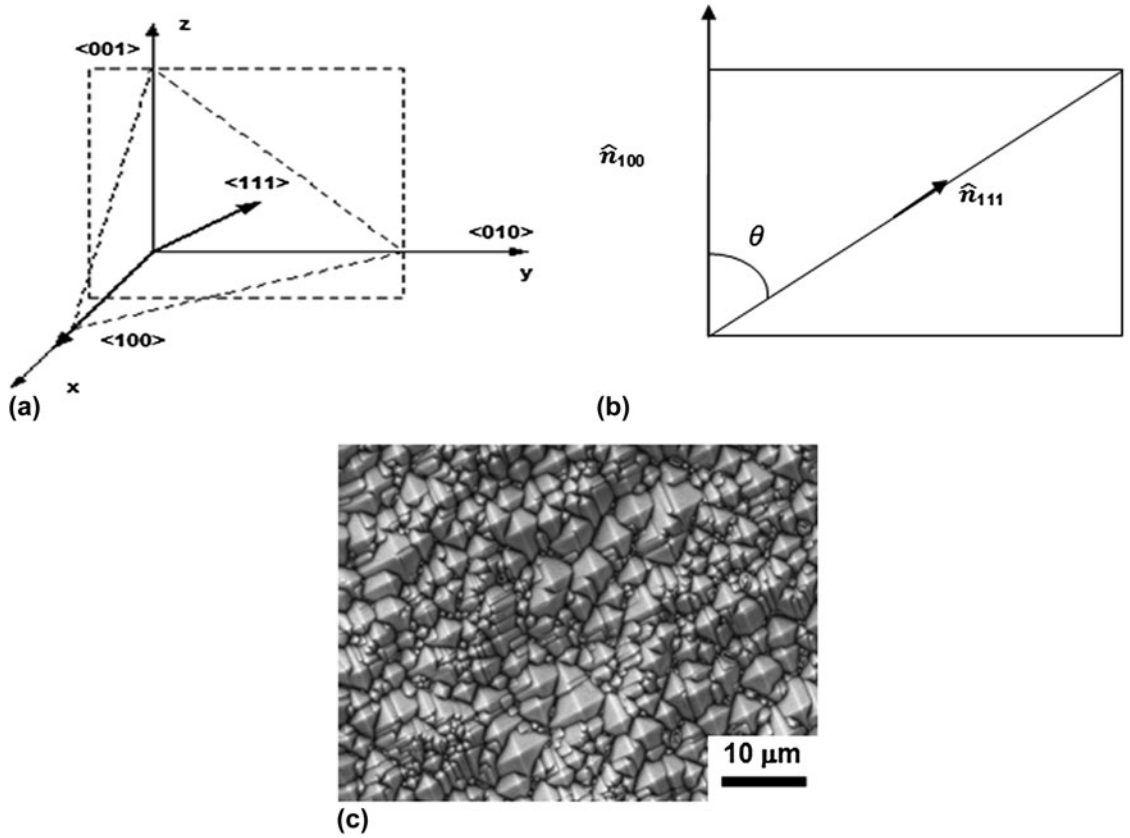


FIG. 1. (a) The square and triangular shapes represent the (100) plane and (111) plane, respectively, (b) a rectangle including the main diagonal of the cube used to determine the angle of interest, and (c) SEM image of pyramids on the surfaces of KOH etched (001) silicon wafers.

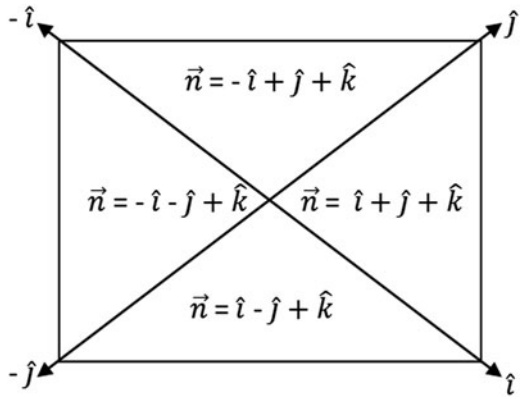


FIG. 2. Top-view of a square based pyramid showing the unit vectors and normal vectors on the textured surface.

except when the incident angle is equal to 0°. When $\theta = 0°$, the light ray vector is defined by $v = -k$.

Once the incident light ray vector is known, the angles of the facets can be determined from Eq. (3). This makes it easier to obtain the secondary reflections. The coordinates of the reflected vector can be determined from the Phong's model.[23] Hence, the angle of incidence of the light reflected from a surface is equal to the angle of reflection, as shown in Fig. 3. If v is the direction of the incidence light ray vector, r is the direction of the reflected ray, n is the surface normal of the substrate, and θ_V and θ_R are the incidence and reflected angles, respectively, the reflected ray vector, r, can be determined from vector projection to be:

$$p = v\frac{|n|}{n} \quad . \tag{4}$$

From Fig. 3, p is a projection of v onto n. Thus, we may rearrange Eq. (4) to obtain:

$$\cos\theta = \frac{|p|}{|v|} \quad . \tag{5}$$

Also, using the dot product of two vectors, we may express cosθ as:

$$\cos\theta = \frac{v\,n}{|v||n|} \quad . \tag{6}$$

https://doi.org/10.1557/jmr.2015.70 Published online by Cambridge University Press

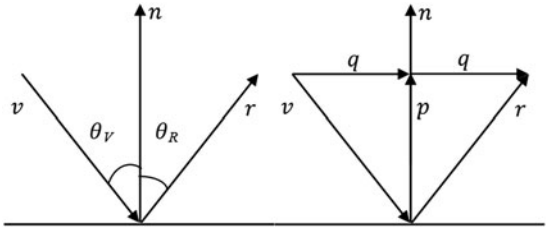


FIG. 3. Phong's reflection model showing the vector projection of the incidence light ray.

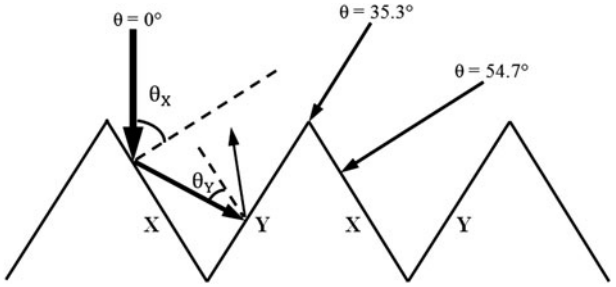


FIG. 4. The schematic diagram of the side view of a periodic pyramidal system.

By combining Eqs. (4)–(6), p becomes

$$p = \frac{v\ n}{|v||n|} n \quad . \tag{7}$$

Since vector q connects v to its projection and also connects p to r, the coordinates of the reflected vector r are given by:

$$r = 2\frac{v\ n}{|v||n|} n - v \quad . \tag{8}$$

As an example, consider the case of light under normal incidence to the substrate, Eq. (8) can be used to calculate the secondary reflection for a given light ray ($v = -k$) that is incident to a facet with $n_1 = i + j + k$. The secondary reflection occurs on a neighboring facet with $n_2 = -i - j + k$. Thus, by combining Eqs. (6) and (8), $\theta = \cos^{-1}\left(5/\sqrt{27}\right)$, which is equal to 15.79°. This implies that, for normal incidence to a textured silicon (100) substrate, all secondary reflections occur at an angle of 15.79°.

The above method represents a possible approach to the determination of the angles between any incoming ray of light and any pyramidal facet. However, it does not treat cases in which fractions of the light rays are incident on different facets. Furthermore, the method does not determine whether reflection actually occurs or not. These issues can be addressed by exploring simpler systems, such as periodic two-dimensional (2D) arrangements of textured pyramids that will be considered in the next section.

2. 2D model of periodic pyramidal structures

a. Basic assumptions

A 2D model of a periodic pyramidal system is illustrated schematically in Fig. 4. This can be achieved in practice by masking the surface of a silicon wafer prior to the etching process.[20] Assuming that the incident light rays are perpendicular to the surface of the substrate, the optical interaction of light (with the separate facets X and Y) can be idealized, as a two-dimensional problem.

In an effort to determine whether the angle of incidence, prior to the primary reflection on surface X, can produce secondary reflections, we gradually increase the angle of incidence from $\theta = 0°$ to $\theta = 35.3°$ until the incident light ray is tangential to facet Y (Fig. 4). Above 35.3°, the reflections from facet Y vanish until $\theta = 54.7°$, at which the incident ray becomes normal to facet X. Furthermore, for incident angles greater than 54.7°, the reflected rays are directed away from the substrate and not toward it. Hence, secondary reflection will not occur for angles of incidence greater than 54.7°.

b. Contributing factors from primary, secondary, and total reflectances

To estimate the total reflectance, the fraction of light rays that is incident to each facet is estimated along with their contributions to the total reflectance. As shown in Fig. 4, angles θ_X and θ_Y are the angles between the light ray and the normal vectors to facets X and Y, for primary reflections. Hence, the fraction of the light ray that falls on each facet can be expressed simply as the ratio of that angle's cosine to the sum of both angles' cosines. This is given by:

$$F_{X1} = \frac{\cos(\theta_X)}{\cos(\theta_X) + \cos(\theta_Y)} \quad F_{Y1} = \frac{\cos(\theta_Y)}{\cos(\theta_X) + \cos(\theta_Y)} \quad , \tag{9}$$

where F_{X1} and F_{Y1} are the contributing factors of the primary reflections from facets X and Y, respectively. Since all of the reflections from facet Y vanish for angles greater that 35.3°, Eq. (9) is only valid for angles, θ, up to 35.3°. Beyond $\theta = 35.3°$, $F_{X1} = 1$ and $F_{Y1} = 0$. For secondary reflections from facet Y, the fractional contributing factor, $F_{Y2} = 1$, since any light ray reflected from facet Y experiences a secondary reflection.

Unlike factor F_{Y2}, the contributing factor (F_{X2}) of the secondary reflections from facet X is more complex.

https://doi.org/10.1557/jmr.2015.70 Published online by Cambridge University Press

By inspection, the contributing factor F_{X2} varies from 1 to 0, for four separate cases in the angle of incidence. In the first case, when the angle of incidence (to the substrate) is less than 19.4°, secondary reflection occurs on the neighboring Y facet, for all light rays that strike any arbitrary point on facet X. Secondly, for angles of incidence between 19.4° and 35.3°, some of the light rays reflected from facet X are directed away from the substrate, while those at angles of incidence between 35.3° and 54.7° are not able to strike some portion of facet X, due to shading from facet Y. Finally, at any angle greater than 54.7°, secondary reflections can no longer occur.

For any angle of incidence between 19.4° and 35.3°, as illustrated in Fig. 5, secondary reflection does not occur between points M and B on facet X (i.e., line length MB). Therefore, the fraction of facet X that does not produce secondary reflections from incident light rays is simply the ratio of the MB to MO. From Fig. 5, the base length of the pyramid is equal to the distance between the peaks of the two pyramids. This implies that MH is twice the line length, a, shown in Fig. 5. Hence, the line length, a, can be related to the side length, L, via the following expression:

$$a = L\cos\theta \quad . \tag{10}$$

Hence, for $\theta = 54.7°$, Eq. (10) gives $a = L\cos(54.7) = L/\sqrt{3}$.

Since MH is twice the length of the line segment, a, MH is now given by:

$$\mathrm{MH} = 2a = 2L/\sqrt{3} \quad .$$

Furthermore, applying the sine rule to triangle HMB, we obtain:

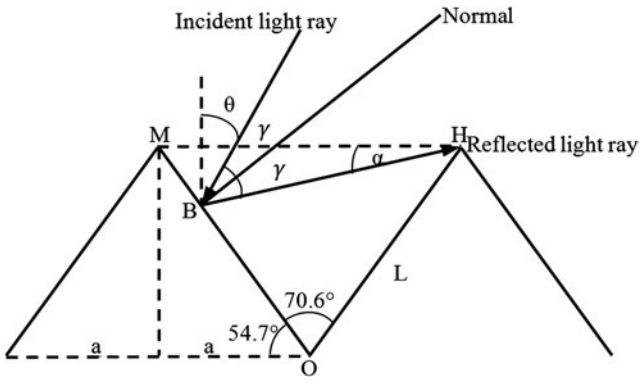


FIG. 5. Light interaction with the pyramid facet at an angle between 19.4° and 35.3°.

$$\frac{\sin(\alpha)}{\mathrm{MB}} = \frac{\sin(125.3 - \alpha)}{\mathrm{MH}} \quad . \tag{11}$$

Substituting $\mathrm{MH} = 2L/\sqrt{3}$ into Eq. (11) now gives:

$$\frac{\sin(\alpha)}{\mathrm{MB}} = \frac{\sin(125.3 - \alpha)}{\frac{2L}{\sqrt{3}}} \quad . \tag{12}$$

Hence, rearranging Eq. (12) now gives:

$$\frac{\mathrm{MB}}{L} = \frac{\frac{2}{\sqrt{3}}\sin(\alpha)}{\sin(125.3 - \alpha)} \quad . \tag{13}$$

Thus, the relationship between the angle of incidence, θ, and the angle, α, opposite to the line length MB, can be obtained by applying the sine rule to triangle MHB. Since the incidence light ray is reflected across the normal to the line MB, we can also equate the included angle to 90°. That gives:

$$\gamma + \theta + 35.3^{\circ} = 90^{\circ} \quad . \tag{14}$$

Rearranging Eq. (14) now gives

$$\gamma = 54.7^{\circ} - \theta \quad .$$

Also, from triangle MCB, we can deduce that:

$$2\gamma + \theta = 90^{\circ} - \alpha \quad . \tag{15}$$

Hence, $2(54.7° - \theta) + \theta = 90° - \alpha$, and α is now given by

$$\alpha = \theta^{\circ} - 19.4^{\circ} \quad . \tag{16}$$

Hence, substituting Eq. (16) into Eq. (13) now gives:

$$\frac{\mathrm{MB}}{L} = \frac{\frac{2}{\sqrt{3}}\sin\left(\theta^{\circ} - 19.4^{\circ}\right)}{\sin\left(144.7^{\circ} - \theta^{\circ}\right)} \quad . \tag{17}$$

https://doi.org/10.1557/jmr.2015.70 Published online by Cambridge University Press

Thus, the contributing factor, F_{X2}, of the secondary reflections for this range is given by:

$$F_{X2} = 1 - \frac{MB}{L} = 1 - \frac{\frac{2}{\sqrt{3}}\sin\left(\theta^{\circ} - 19.4^{\circ}\right)}{\sin\left(144.7^{\circ} - \theta^{\circ}\right)} \quad . \qquad (18)$$

For angles of incidence between 35.3° and 54.7° (Fig. 6), the part of facet X between points O and A (line length OA) does not have access to light rays due to the effects of shading. The proportion of facet X that is not accessible to light rays can thus be expressed as the ratio of the OA to the side length of the pyramid, OM or *L*.

Hence, by applying the sine rule to triangle HOA, we obtain:

$$\frac{\sin(\beta)}{OA} = \frac{\sin(109.4 - \beta)}{L} \quad . \qquad (19a)$$

Rearranging Eq. (19) now gives:

$$\frac{OA}{L} = \frac{\sin(\beta)}{\sin(109.4 - \beta)} \quad . \qquad (19b)$$

Furthermore, by substituting the angle, β, with the expression $\beta = \theta - 35.3°$, we have:

$$\frac{OA}{L} = \frac{\sin\left(\theta - 35.3^{\circ}\right)}{\sin(144.7 - \theta)} \quad . \qquad (20)$$

Thus, the contributing factor, F_{X2}, of the secondary reflections for this range is given by:

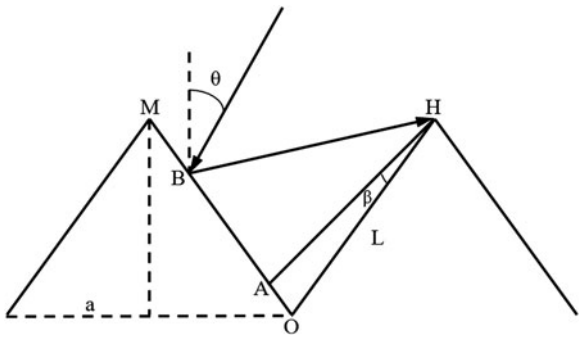


FIG. 6. Light interaction with the pyramid facet at an angle between 35.3° and 54.7°.

$$F_{X2} = 1 - \frac{MB}{L} - \frac{OA}{L} = 1 - \frac{\frac{2}{\sqrt{3}}\sin\left(\theta^{\circ} - 19.4^{\circ}\right)}{\sin\left(144.7^{\circ} - \theta^{\circ}\right)} - \frac{\sin\left(\theta - 35.3^{\circ}\right)}{\sin(144.7 - \theta)} \quad . \qquad (21)$$

So for all angles, F_{X2} can be obtained via any of the following expressions, depending on the range of the angle of incidence of the light rays:

$$F_{X2} = \begin{cases} 1 & \theta \le 19.4^{\circ} \\ 1 - \frac{\frac{2}{\sqrt{3}}\sin\left(\theta^{\circ} - 19.4^{\circ}\right)}{\sin\left(144.7^{\circ} - \theta^{\circ}\right)} & 19.4^{\circ} \le \theta \le 35.3^{\circ} \\ 1 - \frac{\frac{2}{\sqrt{3}}\sin\left(\theta^{\circ} - 19.4^{\circ}\right) + \sin\theta^{\circ} - 35.3^{\circ}}{\sin\left(144.7^{\circ} - \theta^{\circ}\right)} & 35.3^{\circ} \le \theta \le 54.7^{\circ} \\ 0 & \theta \ge 54.7^{\circ} \end{cases} \quad . \qquad (22)$$

By combining the primary and secondary reflections with their contributing factors, the total reflectance can be obtained from the following expression[26,27]:

$$R_T = R_{X1}F_{X1}[R_{X2}F_{X2} + (1 - F_{X2})] + R_{Y1}F_{Y1}R_{Y2} \quad , \qquad (23)$$

where R_{X1} and R_{Y1} are the primary reflection coefficients from facets X and Y, with contribution factors of F_{X1} and F_{Y1}, respectively. R_{Y2} is the secondary reflection coefficient from facet Y. The secondary reflection coefficient from facet X is represented by R_{X2} with its contribution factor being F_{X2}. However, $(1 - F_{X2})$ accounts for the light not subjected to a secondary reflection from facet X. The reflectance, *R*, for both the primary and secondary reflections can be obtained using the Fresnel equations adopted from Ref. 28. These give:

$$R = |r|^2 = \left(\frac{\cos(\theta) - \sqrt{\left(\frac{n_{Si}}{n_{air}}\right)^2 - \sin^2(\theta)}}{\cos(\theta) + \sqrt{\left(\frac{n_{Si}}{n_{air}}\right)^2 - \sin^2(\theta)}} \right)^2 \quad , \qquad (24)$$

where *r* represents the reflection coefficient for both the primary and secondary reflections.

III. EXPERIMENTAL PROCEDURES

In an effort to validate the pyramidal structures used in the above model, the (100)-oriented silicon wafers were

https://doi.org/10.1557/jmr.2015.70 Published online by Cambridge University Press

procured from Semiconductor Wafer Inc., Hsinchu, Taiwan. Prior to alkaline etching, the wafers were dipped in 0.5% HF for 100 s to remove native oxides and subsequently dried in nitrogen gas. Samples were etched in an alkaline solution of KOH under the etching conditions of an etch duration of 40 min, an etch temperature of 80 °C, and a volume concentration of KOH:IPA in the ratio 2:4. Also, at the end of each texturing process, the samples were rinsed in distilled de-ionized water and dried in nitrogen gas.

The alkaline etching was carried out in a GFL-1083 thermo-coupled water bath (Gesellschaft für Labortechnik (GFL), Burgwedel, Hanover, Germany). Scanning electron images of the etched and unetched silicon surfaces were then obtained using an EVO MA-10 scanning electron microscope (SEM) that was operated at 10 kV (EVO MA-10, Carl Zeiss, Hamburg, Germany).

IV. RESULTS AND DISCUSSION

A. Reflection from etched 100 silicon surfaces

A secondary electron image of an etched (100)-oriented silicon wafer surface is presented in Fig. 1. This shows clearly that pyramidal facets are formed on the silicon wafer, after etching. This has geometrical characteristics that are similar to those discussed and idealized earlier in Sec. 2. However, unlike the idealized unit cell structures, in which the pyramidal dimensions were uniform, the actual pyramidal structures exhibited variations in the unit cell heights, although the basic shapes were geometrically similar. The interactions with the incident light rays should, therefore, apply to primary reflections, since the secondary reflections may be affected by differences in the adjacent facets.

As discussed in the preceding section, the possibility that the incident light will experience a secondary reflection (double-bounce incidence) or a multiple reflection depends upon the height of the pyramid, the apex angle of the pyramid, and the facet tilt angles of the geometrical textures, with respect to the surface of the wafer.[29,30] From prior work by Sethi et al.,[31] a secondary reflection is experienced or guaranteed, if the facet tilt angle falls within the range between 45° and 60°. Since texturing of (100)-oriented silicon wafers in the alkaline solution produces pyramids with an apex angle of 70.6° and a facet tilt angle of 54.7° for an ideal process or $<52°$ for a non-ideal process,[16,22] which are within the range specified by Sethi et al.,[31] our model can be used to investigate the possibility of secondary reflection, for the full range of incidence angles to the substrate.

By inspection, when the angle of incidence to the substrate is less than 19.4°, secondary reflection occurs on the neighboring Y facet, for all light rays that strike any arbitrary point on X facet. This validates prior work on the reflection of normally incident light rays using the OPAL 2 software[32,33] to show that 88.9% of incident rays experience a double and 11.1% experience triple bounce. However, if the angle of incidence is between 19.4° and 35.3°, some light is reflected from facet X. The reflected light is directed away from the substrate, leaving only some proportion of the facet to experience secondary reflection.

In the case of incident angles between 35.3° and 54.7°, the incident light rays are not able to strike some portion of facet X. This is due to shading from facet Y. However, for incident angles equal to 54.7°, the possibility of secondary reflections is eliminated because the incident light is perpendicular to facet X. Thus, at any angle greater than 54.7°, secondary reflections cannot occur. Hence, any incident light rays that strike the textured surfaces of etched (001)-oriented silicon surfaces at low incidence angles produce more secondary reflections and thus have at least two chances of being absorbed. However, the chances of absorption are reduced at high incidence angles, where most of the reflected light rays are directed away from the substrate.

B. Total reflectances

It is important to note here that the above model does not account for the tertiary reflections, as with prior work on the reflection of normally incident sunlight.[16,17,22] These were not explored, since they do not occur often for non-normal incident angles.[31] Furthermore, they have only a minor effect on the overall accuracy of the total reflectance.[31] Also, in the 2D textured surface model, the pyramids were assumed to be aligned with one another, as shown in Fig. 4. However, this is valid only for regular inverted pyramidal textures and not for randomly textured silicon wafers. Hence, a more realistic approach is needed to model the light/pyramid interactions in actual etched (001)-oriented silicon wafers with textures similar to those presented in Fig. 1. Nevertheless, the results obtained from the current idealized 2D textured surface model are close to the measured reflectance values presented by Parretta et al.[20]

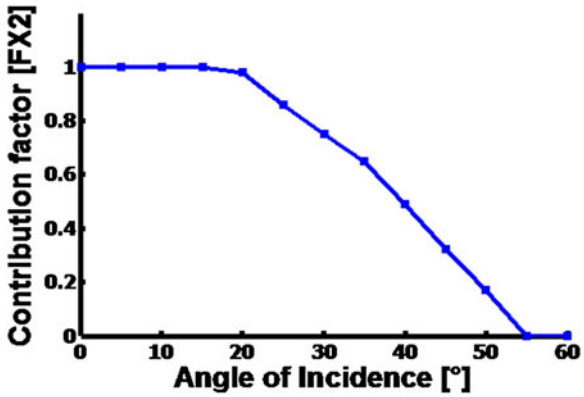


FIG. 7. The dependence of F_{X2} on the incidence angle.

https://doi.org/10.1557/jmr.2015.70 Published online by Cambridge University Press

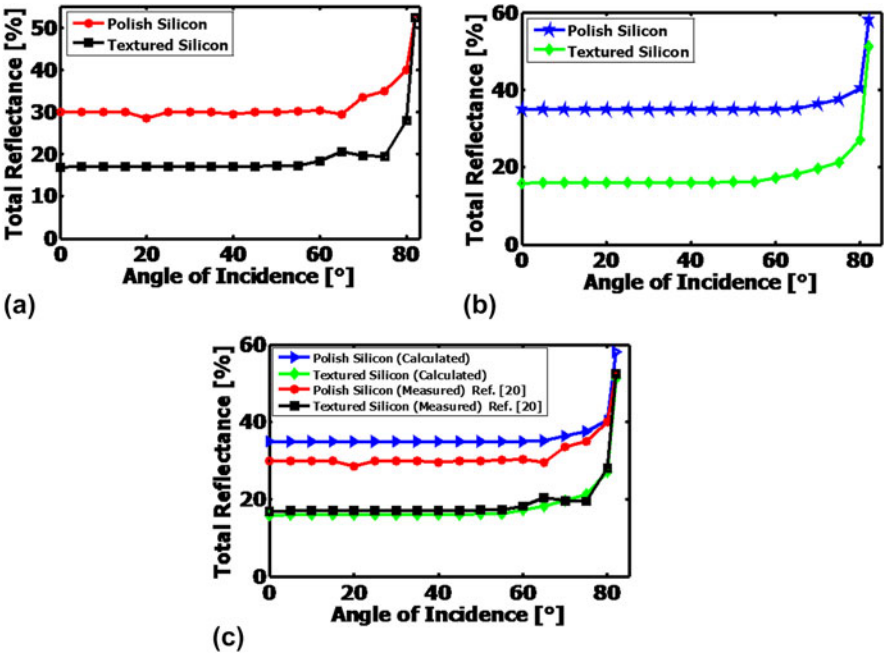


FIG. 8. (a) Measured total reflectance versus angle of incidence treated at $\lambda = 633$.[20] (b) Calculated total reflectance versus angle of incidence treated at $\lambda = 635$. (c)The calculated and measured reflectance versus angle of incidence.

A summary of the contribution factors (F_{X2}) obtained for different angles of incidence is presented in Fig. 7. This shows that, above the incident angle of 19.4°, F_{X2} decreases gradually with increasing angle of incidence. Furthermore, the dependence of the total reflectance on the angle of incidence is presented in Figs. 8(a) and 8(b), for etched (001)-oriented surfaces subjected to incident light rays with a wave length, λ, of 635 nm. In all cases, the total reflectances of the textured surfaces are lower than those of the flat polished surfaces.

The predicted reflectances [obtained from Eq. (23)] are also in good agreement with the measured reflectance values [Fig. 8(c)]. The close agreement between the experimental and predicted reflectances suggests that the idealized model presented here captures most of the important aspects of light interactions with the pyramidal structures that are formed by the alkaline etching of (001)-oriented silicon surfaces with etchants such as KOH.

C. Implications

The implications of the above model are quite significant. First, they show that more secondary reflections are experienced on textured silicon (100)-oriented wafers at low incidence angles. The optical path lengths also increase with increasing secondary reflections, thus, providing increased chances of light absorption. This suggests that KOH textured pyramidal structures can be tailored to control their reflectance, when the angle of incidence of light and the uniformity of the pyramids are well controlled.

Furthermore, the good agreement between the measured and the predicted reflectances suggests that our 2D model captures most of the important aspects of light interactions with the pyramidal structures that are formed by the KOH-etching of (001)-oriented silicon surfaces.

These resulting reductions in surface reflectance enable more light to be trapped for conversion to charge in single crystal silicon solar cells. The control of alkaline etching can, therefore, be used to engineer the improvement of silicon solar cell efficiency. Further work is clearly needed to explore the possible improvements in solar cell efficiency that can be achieved via the controlled alkaline etching of silicon wafers in silicon solar cells.

V. CONCLUSIONS

(1) A simple analytical model has been developed and used to study the optical behavior of flat and textured silicon substrates. The model explored the possibility of secondary reflections, for the full range of incidence angles to the silicon substrate. The geometrical interactions of light rays with pyramidal facets were used to predict the reflectance values, which were compared with measurements of reflectance on alkaline textured silicon surfaces.

(2) Secondary reflection is experienced or guaranteed, for all pyramid heights, when the angle of incidence to the substrate is less than 19.4°. Hence, any incident light beams that strike the textured surfaces of etched (001)-oriented silicon surfaces at low incidence angles produce more secondary reflections than flat silicon

https://doi.org/10.1557/jmr.2015.70 Published online by Cambridge University Press

substrates. Thus, secondary reflections increase the time available for the incident light rays to be absorbed into (001)-oriented silicon single crystals.

(3) The predictions obtained from the current 2D textured surface model are close to the measured reflectance values presented in Ref. 20. The close agreement between the experimental and predicted reflectances suggests that the idealized model presented here captures most of the important aspects of light interactions with the pyramidal structures that are formed by the alkaline etching of (001)-oriented silicon surfaces with etchants such as KOH.

(4) The current results suggest that the model can be helpful in the design of textured silicon surfaces for the control of surface reflectance and the trapping of light by secondary reflections. Such control and trapping could lead to increased photoconversion and silicon solar cell efficiency.

ACKNOWLEDGMENTS

The authors are grateful to thank Prof. Oleg Yordanov, Bruno Dandogbessi, and Uche Opara for useful scientific discussions. Appreciation is also extended to the World Bank STEP-B Program, the World Bank African Centers of Excellence Program, the African Development Bank, the African Capacity Building Foundation (ACBF), and the Nelson Mandela Institute for financial support.

REFERENCES

1. H. Chung, C. Chen, and H. Chu: Analysis of pyramidal surface texturization of silicon solar cells by molecular dynamics simulations. *Int. J. Photoenergy* **2008**, 1–6 (2008).
2. J.M. Gee, R. Gordon, and H.F. Laing: Optimization of textured-dielectric coatings for crystalline-silicon solar cells. In *Proceedings of the 25th IEEE Photovoltaic Specialists Conference, Washington DC*, 1996; pp. 733–736.
3. J.D. Hylton, A.R. Burgers, and W.C. Sinke: Alkaline etching for reflectance reduction in multicrystalline silicon solar cells. *J. Electrochem. Soc.* **151**(6), 408–427 (2004).
4. C.R. Tellier and A. Brahim-Bounab: Anisotropic etching of silicon crystals in KOH solution. *J. Mater. Sci.* **29**(22), 5953–5971 (1994).
5. M. Shikida, K. Sato, K. Tokoro, and D. Uchikawa: Differences in anisotropic etching properties of KOH and TMAH solution. *Sens. Actuators, A* **80**, 179–188 (1999).
6. H. Seidal, L. Csepregi, A. Henberger, and H. Baumgartel: Anisotropic etching of crystalline silicon in alkaline solutions. *J. Electrochem. Soc.* **137**(11), 116–125 (1990).
7. P. Kilpinen, E. Haimi, and V.K. Lindroos: The etch rate variations of p+ silicon wafers in aqueous KOH solutions as a function of processing conditions. *MRS Proc.* **605**, 293 (1999). doi:10.1557/PROC-605-293.
8. H. Seidal, L. Csepregi, A. Henberger, and H. Baumgartel: Anisotropic etching of crystalline silicon in alkaline solution: Orientation dependence and behavior of passivation layers. *J. Electrochem. Soc.* **137**(11), 612–626 (1996).
9. K. Sato, M. Shikida, T. Yamashiro, M. Tsunekawa, and S. Ito: Roughening of single-crystal silicon surface etched by KOH water solutions. *Sens. Actuators, A* **73**, 122–130 (1999).
10. L.E. Kassel: KOH-etch related defects on processed silicon wafers. *MRS Proc.* **259**, 187 (1992). doi:10.1557/PROC-259-187.
11. C. Yang, P. Chen, Y. Chiou, and R. Lee: Effects of mechanical agitation and surfactant additive on silicon anisotropic etching in alkaline KOH solution. *Sens. Actuators, A* **119**, 263–270 (2005).
12. I. Zubel and M. Kramkowska: The effect of isopropyl alcohol on etching rate and roughness of (100) Si surface etched in KOH and TMAH solutions. *Sens. Actuators, A* **93**, 138–147 (2001).
13. V. Moroz, J. Huang, K. Wijekoon, and D. Tanner: Experimental and theoretical analysis of the optical behavior of textured silicon wafers. In *Proceedings of the 37th IEEE Photovoltaic Specialists Conference*. (IEEE, Seattle, WA, 2011); pp. 2900–2905.
14. X. Zhu, L. Wang, and D. Yang: Investigations of random pyramid texture on the surface of single-crystalline silicon for solar cells. In *Proceedings of the ISES Solar World Congress*, Beijing, China, (Springer-Verlag, Berlin Heidelberg, Germany, 2007); pp. 1126–1130.
15. P. Campbell and M.A. Green: Light trapping properties of pyramidally textured surfaces. *J. Appl. Phys.* **62**(1), 243–249 (1987).
16. S.C. Baker-Finch and K.R. McIntosh: Reflection distributions of textured monocrystalline silicon: Implications for silicon solar cells. *Prog. Photovoltaics Res. Appl.* **21**(5), 960–971 (2013). DOI: 10.1002/pip.2186.
17. S.C. Baker-Finch and K.R. McIntosh: Reflection of normally incident light from silicon solar cells with pyramidal texture. *Prog. Photovoltaics Res. Appl.* **19**(4), 406–416 (2011). DOI: 10.1002/pip.1050.
18. W.C. O'Mara, R.B. Herring, and L.P. Hunt: *Handbook of Semiconductor Silicon Technology* (William Andrew Inc., Norwich, NY, 1990); pp. 349–352.
19. D.L. King and M.E. Buck: Experimental optimization of an anisotropic etching process for random texturization of silicon solar cells. In *Proceedings of the 22nd IEEE Photovoltaic Specialists Conference*, 1991; pp. 303–308.
20. A. Parretta, A. Sarno, P. Tortora, H. Yakubu, P. Maddalena, J. Zhao, and A. Wang: Angle dependent reflectance measurements on photovoltaic materials and solar cells. *Opt. Commun.* **172**(1–6), 139–151 (1999).
21. J.A. Dziuban: *Bonding in Microsystem Technology* (Springer, Science & Business Media, 2007); p. 16.
22. S.C. Baker-Finch: Rules and tools for understanding, modelling and designing textured silicon solar cells. Ph.D. Thesis, Australia National University, 2012.
23. B. Geitz: *Vector Geometry for Computer Graphics*. e-Publishing, Part III (2007); pp. 15–16. [Online]. Available: https://cs.oberlin.edu/~bob/cs357.08/VectorGeometry/VectorGeometry.pdf (Accessed August 25, 2013).
24. K. Wijekoon, T. Weidman, S. Paak, and K. MacWilliams: Production ready novel texture etching process for fabrication of single crystalline silicon solar cells. In *Proceedings of the 35th IEEE Photovoltaic Specialists Conference*, Honolulu, HI, 2010; pp. 3635–3641.
25. P.M.M. Bressers, J.J. Kelly, J.G.E. Gardeniers, and M. Elwenspoek: Surface morphology of p-type (100) silicon etched in aqueous alkaline solution. *J. Electrochem. Soc.* **143**(5), 1744–1750 (1996).
26. C.J. Wu, P.J. Wei, and J.F. Lin: The reflectivity of an etched silicon surface with pyramids: I. Theoretical model and its predictions. *J. Micromech. Microeng.* **19**, 1–7 (2009).
27. P.K. Singh, R. Kumar, M. Lal, S.N. Singh, and B.K. Das: Effectiveness of anisotropic etching of silicon in aqueous alkaline solution. *Sol. Energy Mater. Sol. Cells* **70**, 102–113 (2001).
28. F.L. Pedrotti, L.S. Pedrotti, and L.M. Pedrotti: *Introduction to Optics*, 3rd ed. (Pearson Prentice Hall, Upper Saddle River, NJ, 2007).

https://doi.org/10.1557/jmr.2015.70 Published online by Cambridge University Press

29. A. Hamel and A. Chibani: Characterization of texture surface for solar cells. *J. Appl. Phys.* **10**(3), 231–234 (2010).
30. Z. Xi, D. Yang, W. Dan, C. Jun, X. Li, and D. Que: Texturization of cast multicrystalline silicon for solar cells. *Semicond. Sci. Technol.* **19**(3), 485–489 (2004).
31. C. Sethi, V.K. Anand, K. Walia, and S.C. Sood: Optimization of surface reflectance for alkaline textured monocrystalline silicon solar cell. *IJCSCT* **5**(1), 785–788 (2012).
32. K.R. McIntosh and S.C. Baker-Finch: OPAL 2: Rapid optical simulation of silicon solar cells. In *Proceedings of the 38th IEEE Photovoltaic Specialists Conference*, Austin, TX, 2012; pp. 265–271. DOI: 10.1109/PVSC.2012.6317616.
33. S.C. Baker-Finch and K.R. McIntosh: A freeware program for precise optical analysis of the front surface of a solar cell. In *Proceedings of the 35th IEEE Photovoltaic Specialists Conference*, Honolulu, HI, 2010; pp. 2184–2187. DOI: 10.1109/PVSC.2010.5616132.

https://doi.org/10.1557/jmr.2015.70 Published online by Cambridge University Press